ELSEVIER

Water Research 38 (2004) 2095–2102

WATER RESEARCH

www.elsevier.com/locate/watres

Salt tracer experiments in constructed wetland ponds with emergent vegetation: laboratory study on the formation of density layers and its influence on breakthrough curve analysis

Bernhard H. Schmid[a,*], Michael A. Hengl[b], Ursula Stephan[b]

[a] *Institut für Hydraulik, Gewässerkunde und Wasserwirtschaft, Technische Universität Wien, clo Vegagasse 16, Vienna A-1190, Austria*
[b] *Institut für Wasserbau und hydrometrische Prüfung, Severingasse 7, Vienna A-1090, Austria*

Received 11 July 2003; received in revised form 10 December 2003; accepted 22 January 2004

Abstract

Constructed wetlands are a rapidly expanding and intensively studied wastewater treatment system. One of the main types in use is the free water surface (FWS) wetland or wetland pond. In studies on these ponds, salt tracer experiments are a convenient tool to determine travel time distributions, which are, in turn, related to hydraulic and sedimentation (trapping) as well as nutrient removal efficiencies. Typically, flows encountered in constructed wetland ponds are characterized by low Reynolds numbers, at times even within the laminar flow regime. In such conditions the injection of salt may cause strong density effects, thereby threatening the usefulness of the recorded breakthrough curves. The processes and mechanisms governing the formation of density stratification due to salt tracer injections into wetland ponds with emergent vegetation were studied in the laboratory. The results reported are expected to be useful in the planning of future field tracer experiments.

Keywords: Constructed wetlands; Salt tracers; Density effects; Mixing energy; Breakthrough curve; Tracer tests

1. Introduction

For the past two decades, constructed wetlands have been among the most rapidly expanding wastewater treatment systems [1]. Worldwide, studies are being conducted into the mechanisms and processes active in these wetlands, aiming at a better understanding and improvement of performance. In terms of their hydraulic characteristics, the following kinds of constructed wetlands are distinguished: the wetland pond or free water surface (FWS) type, the groundwater flow (GWF) type with a porous media passage and the combined overland and groundwater flow (OGF) type. It is the first of these three types mentioned, the wetland ponds, that will be addressed here.

Salt tracer experiments are a convenient and widespread method for use in studies on constructed wetland ponds. The removal efficiency and effectiveness of the wetland ponds is considered to be strongly related to the distribution of flow or travel times in the pond, the ideal often being plug flow conditions (deviations from which may depend on a number of factors, among which the pond form is of importance [2]). The distribution of flow paths is, in turn, reflected by concentration–time distributions or breakthrough curves of an ideal tracer injected into the flow. Thus, it is only natural that tracer experiments are frequently used to study travel time distributions and flow paths, thereby hoping to obtain indications of hydraulic and removal efficiency. Tracers available range from various salts (like KBr) over dyes (such as Rhodamin WT) to radioactive substances (primarily tritium) and, most recently, artificially produced pieces of DNA chains [3]. Dye tracers may be subject to photochemical decay, adsorption and

*Corresponding author.
E-mail address: schmid@hydro.tuwien.ac.at (B.H. Schmid).

0043-1354/$ - see front matter
doi:10.1016/j.watres.2004.01.038

Nomenclature

B	flume width (m)
C	salt concentration ($mg\,l^{-1}$)
C_0	initial salt concentration ($mg\,l^{-1}$)
C_{max}	maximum initial salt concentration without notable density effects ($mg\,l^{-1}$)
c_{max}	dimensionless maximum initial salt concentration (dimensionless)
C_D	drag coefficient (dimensionless)
d	stem diameter (m)
f	dimensionless coefficient related to the vertical mixing energy (dimensionless)
F_D	force per unit length of a stem ($N\,m^{-1}$)
E_v	energy for vertical displacement (Nm)
g	acceleration of gravity ($m\,s^{-2}$)
h	water depth (m)
M_0	mass of salt injected (g)
n	number of stems (dimensionless)
q	discharge per unit width ($m^2\,s^{-1}$)
Q	flow rate ($m^3\,s^{-1}$)
Re	Reynolds number (dimensionless)
Re^*	stem Reynolds number (dimensionless)
S	salinity (ppt)
T	temperature (°C)
u	velocity component in streamwise direction ($m\,s^{-1}$)
u_0	approach velocity ($m\,s^{-1}$)
V	volume of saline water after full initial mixing of salt with the inflow (m^3)
W	work done to move the water past the stems (Nm)
W_1	work done to move the water past one single stem (Nm)
x	streamwise coordinate (m), positive in flow direction
z	vertical coordinate (m), positive upwards

Greek letter

ΔL	distance between inflow and measuring cross-sections (m)
Δt	duration of pulse injection (s)
ν	kinematic viscosity ($m^2\,s^{-1}$)
ρ	fluid density ($kg\,m^{-3}$)

biodegradation [4] potentially resulting in low recovery rates [5], whereas tritium (though it probably comes closest to an ideal tracer) cannot be generally used due to a restrictive permitting policy in some European countries. If permitted, radioactive tracers require specialist injection and detection equipment, and their use may arouse public disquiet [6]. Consequently, the tracers most commonly used in wetland studies are salts, which are cheap, largely inert and typically not hazardous. Users of salt tracers, however, run the risk of having their results compromised by density effects, especially in cases of slow to nearly stagnant flows at Reynolds numbers of 1000 or less, and it is just this flow regime which is typical of wetland ponds [1,7]. In this context, it is the purpose of the study presented here to contribute to an improved knowledge of the conditions governing density stratification due to salt tracer injections into wetland ponds with emergent vegetation.

2. Experimental set-up and methodology

The development of salt-induced density stratification was studied experimentally in a 1.5 m wide and some 40 m long, straight recirculating laboratory flume of rectangular cross-section with smooth (cement-coated) floor and walls. Artificial vegetation in the form of emergent plastic tubes of diameter 3.2 cm was placed in the flume at densities 12.8 and 7.0 stems m^{-2} (density 12.8 stems m^{-2} is shown in Fig. 1). The artificial stem diameters were chosen to reflect the hydraulically effective stem diameter typical of *Typha latifolia* (stem together with closely attached leaves measuring some 2–4 cm), and the stem densities relate to loose stands of that plant (between a minimum initial density of about 1 plant m^{-2} [1], and the value for dense cattail stands of slightly above 40 stems m^{-2}, as e.g. measured at Hovi, Finland [8]).

In the experiments the Reynolds numbers, $Re = u \cdot h/\nu$ (with u streamwise velocity, h water depth and ν kinematic viscosity) ranged between some 480 and

Fig. 1. Laboratory flume with 12.8 stems of artificial vegetation m^{-2}.

1300 and two different water depths h (20 and 50 cm, resp.) were studied. These Reynolds numbers were chosen to fall within the range typical of real-world wetlands (see previous section), and water depths of 20–50 cm are also frequently encountered in the field. Reynolds numbers Re below 500 indicate a laminar regime, at Re above 2000 the flow is usually turbulent, with a transition taking place in the interval $500 < Re < 2000$. Thus, the flow regime in constructed wetland ponds is predominantly laminar or (nearly laminar) transitional, and this had to be reproduced in the laboratory experiments.

Velocities were measured by means of a 3D Acoustic Doppler Velocimeter (ADV) operating at 10 MHz acoustic frequency with a velocity resolution of $0.1\,\mathrm{mm\,s^{-1}}$, and the velocity range was set to $\pm 0.03\,\mathrm{m\,s^{-1}}$. The instrument measures in a small sampling volume of less than $0.25\,\mathrm{cm^3}$ at a point 5 cm away from the sensors, here with a sampling rate set to 10 Hz.

A uniform distribution of inflow over the channel width was achieved by an inflow weir with a horizontal crest (Fig. 2).

To obtain an indication of the importance of wind-induced mixing, three out of the 18 experimental runs reported here were conducted with simultaneous wind shear, with the following wind velocities 10 cm above the water level: $2.4\,\mathrm{m\,s^{-1}}$ in flow direction, 0.5 and $2.4\,\mathrm{m\,s^{-1}}$ against flow direction.

Salt tracer of mass M_0 was injected in the form of a pulse of duration Δt into the inflow of rate Q, resulting in a fully mixed concentration of

$$C_0 = \frac{M_0}{Q \cdot \Delta t}. \quad (1)$$

The salt tracer used was sodium chloride, although trial runs (not reported here) were also made with potassium bromide. Breakthrough curves were measured by electric conductivity probes, and the electric conductivity values obtained were then converted to chloride or bromide concentrations by using calibration curves. This technique was chosen as it permits continuous records to be obtained. The concentration versus conductivity relationships proved quite stable, with very little scatter ($R^2 \approx 0.999$). As the authors' calibration curves demonstrated the electric conductivity of a dilute aqueous solution to change more rapidly with chloride than with bromide concentration [$\mathrm{mg\,l^{-1}}$] (thus making the conversion for chloride more accurate), the chloride tracer was given preference.

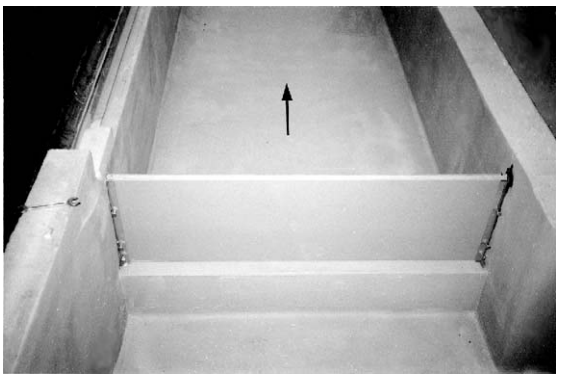

Fig. 2. Picture of broad-crested inflow weir.

Electric conductivity meters were mounted at $x = 34.15$ m (near centreline) at fixed distances from the flume bottom (for water depth $h = 20$ cm: $z = 1.5$, 5, 10 and 15 cm; for $h = 50$ cm: $z = 1.5$, 5, 15, 30 and 48 cm), and this type of set-up was used for all runs listed in Table 1. For an example of the breakthrough curves recorded at $x = 34.15$ m see Fig. 3.

The occurrence of a density stratification can be noted by observing certain properties of the breakthrough curves. In case of a steady injection, density effects are recognizable from a non-uniform distribution of plateau concentrations versus depth, whereas short pulse injections will be associated with non-uniform concentration distributions due to velocity differences over the water depth anyway, i.e. also in cases of neutrally buoyant solute transport. However, the zeroth moments (area under the curve) of concentration versus time distributions will be equal in well-mixed conditions [9], a fact that forms the basis of most discharge measurements by the tracer dilution technique. Table 2 summarizes the normalized zeroth moments of the pulse injection experiments, with the breakthrough curves measured at the depths given above. Normalization was done to facilitate comparison of uniformness or non-uniformness among the various experiments. The 'areas' under the breakthrough curves of each run were scaled such that the average of the (4 or 5) values for each run becomes unity. Visual inspection of the breakthrough curves generated in these experiments suggested the borderline between negligible and non-negligible density effects to be defined by a deviation of the highest or lowest normalized zeroth moment from the mean by an amount of 15–30%. Thus, Table 2 is to be read like this: taking Run 8 as an example, we have normalized zeroth moments decreasing from 1.96 closest to the bottom (most of the salt passed the lowest conductivity probe) to 0.46 at the uppermost measuring point (closest to the water surface). Due to the normalization, the arithmetic mean of the 4 values listed (i.e. 1.96, 0.78, 0.81 and 0.46) is 1.00 (disregarding possible rounding errors) so that the deviation percentages can be seen at a glance. In the case of the example Run 8, the maximum zeroth moment is 96% above the mean, the minimum value is $100-46\% = 54\%$ below the average. By the above definition of a borderline case (maximum roughly

Table 1
Overview of characteristic data

Run no.	Stems (m^{-2})	h (cm)	Temp. (°C)	Q ($l\,s^{-1}$)	q ($m^2\,s^{-1}$)	v-Wind ($m\,s^{-1}$)	Re	Re^*	C_0 ($mg\,l^{-1}$)
1	12.8	20.0	14.7	1.6	0.00107	0.0	924	148	10.8
2	12.8	20.0	15.3	1.6	0.00107	0.0	939	150	14.3
3	12.8	20.0	14.9	1.6	0.00107	0.0	929	149	19.8
4	12.8	20.0	15.1	1.6	0.00107	0.0	934	149	66.9
5	12.8	20.0	15.4	1.6	0.00107	0.0	941	151	71.8
6	12.8	20.0	14.8	1.6	0.00107	0.0	927	148	127.4
7	12.8	20.0	15.9	1.6	0.00107	0.0	953	153	139.7
8	12.8	20.0	16.0	0.8	0.00053	0.0	478	76.4	43.4
9	12.8	20.0	16.0	0.8	0.00053	0.0	478	76.4	86.0
10	12.8	50.0	15.1	1.6	0.00107	0.0	934	59.8	117.2
11	12.8	50.0	14.9	1.6	0.00107	+2.4	929	59.5	125.6
12	12.8	50.0	15.0	1.6	0.00107	−0.5	931	59.6	129.5
13	12.8	50.0	15.1	1.6	0.00107	−2.4	934	59.8	132.0
14	7.0	20.0	15.7	1.6	0.00107	0.0	948	151.7	57.1
15	7.0	20.0	15.8	1.6	0.00107	0.0	951	152.1	73.9
16	7.0	20.0	16.1	0.8	0.00053	0.0	479	76.6	15.0
17	0.0	20.1	21.5	1.6	0.00126	0.0	1289	—	14.3
18	0.0	20.0	21.0	1.6	0.00126	0.0	1274	—	64.9

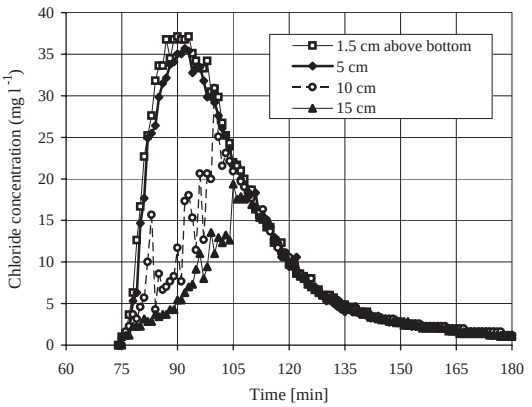

Fig. 3. BTCs, measured 34.15 m from injection, Run 7.

between 1.15 and 1.30, minimum between some 0.70 and 0.85) Run 8 is, consequently, to be classified as a case of distinct density stratification.

3. Results and discussion

Table 1 gives an overview of the tracer experiments presented here, 18 in total. Thirteen experiments were run with stem density $12.8\,m^{-2}$ (out of which three addressed the additional influence of wind) and three more had a lower stem density of $7.0\,m^{-2}$. For comparison, two further runs (numbers 17 and 18, resp.) without stems have been listed. The values of C_0 shown in Table 1 were computed from Eq. (1), and measures were taken to ensure that full initial vertical mixing did actually take place (injection into inflow weir overfall). Duration of injection pulse Δt was 10 min throughout.

Besides $Re = u \cdot h/v$ a further parameter $Re^* = u \cdot d/v$ that could be termed a 'stem Reynolds number' (with stem diameter d as characteristic length in place of water depth h) was added in a separate column of Table 1. In all cases the artificial vegetation consisted of fully emergent, rigid stems (plastic tubes) without leaves. q stands for discharge per unit width.

The stems had a considerable effect on both flow pattern and salt mixing. The distribution of measured streamwise velocities was flatter both in vertical and in transverse direction as compared to corresponding situations without stems. In spite of low vertical changes in these velocities, mixing affected by the presence of the emergent stems was observed to be considerably stronger than without vegetation. So, for instance, Run 2 with 12.8 stems m^{-2}, initially mixed concentration $C_0 = 14.3\,mg\,l^{-1}$, $Q = 1.61\,s^{-1}$ and $h = 20$ cm was repeated without vegetation (Run 17): while this counterpart run without stems produced a borderline case with a still weak, but clearly discernible layering, not the least sign of stratification was observed for Run 2, and this situation essentially persisted in all related runs with stems up to an almost ten-fold concentration C_0 of some $135\,mg\,l^{-1}$ (borderline between the $127.4\,mg\,l^{-1}$ of Run 6 and the $139.7\,mg\,l^{-1}$ of Run 7).

The enhancement of vertical mixing due to the presence of vegetation is confirmed by the pair of experiments with the results shown in Fig. 4: Run 4 with 12.8 stems m^{-2} is associated with practically fully mixed conditions, having zeroth moments at the four depths

Table 2
Normalized zeroth moments at different depths above bottom

Run no.	Depth above bottom (cm)					Stratification
	1.5	5	10	15		Observed
1	0.95	1.04	0.88	1.13		No
2	0.94	0.96	0.99	1.10		No
3	0.99	1.04	0.93	1.04		No
4	1.06	1.04	0.94	0.96		No
5	1.06	1.05	0.95	0.94		No
6	1.12	1.06	0.90	0.92		No/borderline
7	1.28	1.22	0.85	0.66		Yes
8	1.96	0.78	0.81	0.46		Yes
9	2.37	0.87	0.44	0.31		Yes
14	1.05	1.08	0.94	0.92		No
15	1.23	1.18	0.95	0.64		Yes/borderline
16	2.00	0.92	0.57	0.50		Yes
17	1.27	0.79	0.91	1.04		Borderline
18	2.65	0.99	0.28	0.09		Yes
Run no.	Depth above bottom (cm)					Stratification
	1.5	5	15	30	48	Observed
10	Zeroth moments not available due to truncated recession limbs					Yes
11	1.05	1.01	1.00	0.97	0.98	No
12	1.56	1.37	0.69	0.73	0.65	Yes
13	1.01	1.01	1.01	0.99	0.98	No

measured that differ from the mean (normalized: 1.000) by as little as $\pm 6\%$. In contrast, the strongly stratified condition characterising Run 18 can be seen clearly from the plots already: by far most of the salt is contained in the lower half of the water depth, and the respective breakthrough curves at the four depths differ notably from one another.

In fluid dynamics, the patterns and phenomena observed in flow around circular cylinders are related to the Re^* number defined above (and listed in Table 1) as $Re^* = u_0 \cdot d/\nu$, with u_0 the approach velocity, d the diameter and ν the kinematic viscosity of the fluid (water). It is to be noted, however, that the situation treated here differs somewhat from the one typically described in textbooks on fluid mechanics (e.g. [10]) in that the flow is bounded by the flume bottom and the water surface, there is a non-uniform velocity distribution instead of a constant approach velocity, and there is not just one circular cylinder in an otherwise undisturbed flow, but an array of artificial stems affecting the flow and wake patterns. In spite of these differences, it is helpful to summarize a few results from the case of 'one cylinder in a uniform flow'.

For $Re^* \ll 1$, the flow around the cylinder (in an infinite domain) remains symmetrical upstream and downstream, and there is no flow separation [10]. Interpreted within the framework of the experiments reported here, this would mean an approach flow velocity of less than $0.04\,\mathrm{mm\,s^{-1}}$ or (with 1.5 m width and 20 cm depth) a discharge below 11 ml per second, i.e. a practically stagnant pool not really within the range of meaningful tracer experiments in this context. As Re^* is increased, the above-mentioned upstream–downstream symmetry disappears, and for $Re^* > 4$, two attached eddies exist behind the cylinder [10]. Above Re^* of some 40, an unsteady wake region with a vortex street develops, and periodic eddy shedding occurs for $Re^* > 100$. Above Re^* of some 200, and again above some 400, further types of instabilities develop, but the broad picture remains largely the same up to $Re^* \approx 3 \times 10^5$, which is already far beyond the range of interest here. The values from Table 1 place the experiments reported here in the Re^* range above 40 and below 200, and the general observations made agree with the above description. A wake region was found to exist behind the individual cylinders, and mixing was strongly enhanced by the presence of the stems.

An energy argument was applied to derive a semi-quantitative description of the salinity-induced density stratification in these flume experiments with artificial vegetation. The derivation starts from the assumption that the enhancement of mixing by the stems will be in

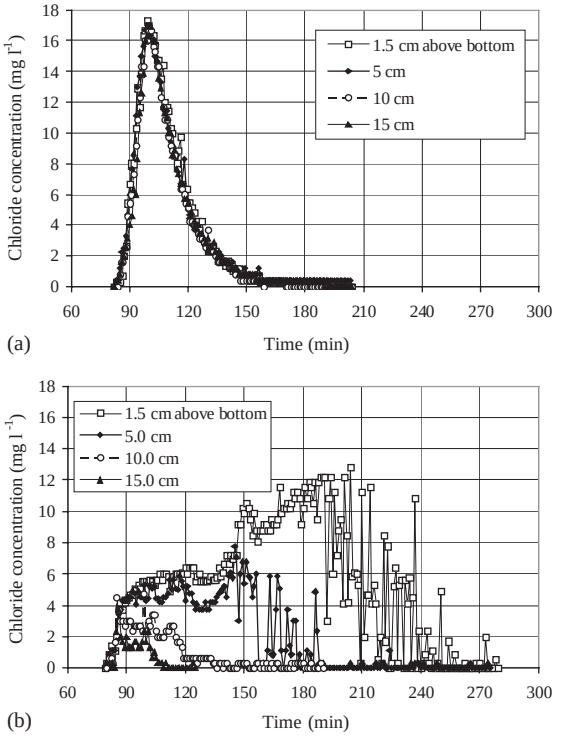

Fig. 4. Comparison of BTCs for $Q = 1.61\,s^{-1}$, $h = 20\,cm$ and $C_0 \approx 66\,mg\,l^{-1}$: (a) with stems (Run 4: 12.8 stems m^{-2}) and (b) without stems (Run 18).

some way related to the work performed by the flow against the resistance of these obstacles. This becomes still more plausible, if one imagines the water to be at rest, with the stems pulled through the pond like a giant brush. To move a single stem through the water for a distance ΔL, work W_1 must be done to the amount

$$W_1 = F_D h \Delta L, \tag{2}$$

with F_D the force per unit length of stem. Assuming that n times this work is required to move n stems through the water (or, conversely, to move the water past n stems at rest), one obtains

$$W = n F_D h \Delta L. \tag{3}$$

It is clear that this linearity assumption underlying Eq. (3) must be justified by comparison with the data, as it is not obvious a priori to what extent the force acting on a single stem will be affected by interaction of vortex streets behind an array of obstacles. Results by Jordanova and James [11] indicate that, for the variation in n treated in the experiments described below (12.8 and 7.0 stems m^{-2}, resp.), the associated change in F_D will be small. Consequently, F_D is expressed here as

$$F_D = C_D \tfrac{1}{2} \rho u_0^2 d, \tag{4}$$

with C_D the drag coefficient, the value of which is a function of Re^*. An empirical relationship for this functional dependence was developed in analogy to the one proposed by Schiller and Naumann [12] and listed in Raudkivi [13] for spherical obstacles. Data compiled by Tritton [10] were used to determine the coefficients to be employed for cylindrical obstacles with the following result, valid for Re^* between 0.1 and 200:

$$C_D = \frac{8}{Re^*}(0.52 + 0.843 Re^{*0.61}). \tag{5}$$

Results from Eq. (5) are shown in Fig. 5 together with data taken from [10]. One can see that the representation is fairly good within the range of applicability given above. At the low Re^* end Eq. (5) approaches

$$C_D \propto \frac{1}{Re^*} \tag{6}$$

and, thus, a linear proportionality of the drag to the velocity, which is a characteristic behaviour at low velocities.

Substitution of Eqs. (5) and (4) into Eq. (3) yields after rearrangement

$$W = n \Delta L \tfrac{1}{2} v \rho q 8(0.52 + 0.843 Re^{*0.61}). \tag{7}$$

The energy required to lift the heavier salt plume by Δz is (see also [14])

$$E_v = g \Delta \rho V \Delta z, \tag{8}$$

with the volume of the saline water $V = Q\Delta t$ (flow rate times injection interval).

The density is related to salinity and temperature by [15]

$$\rho(T, C) = 10^3 + 28.14 - 0.0735T - 0.00469T^2 + (0.802 - 0.002T)(S - 35), \tag{9}$$

with density $\rho[kg\,m^{-3}]$, temperature T [°C] and salinity S [ppt] $\approx$ salt concentration $C[g\,l^{-1}] = 10^{-3} C[mg\,l^{-1}]$ for the dilute solutions treated here. A relative change in ρ due to a change in salt concentration of $\Delta C[mg\,l^{-1}]$ then

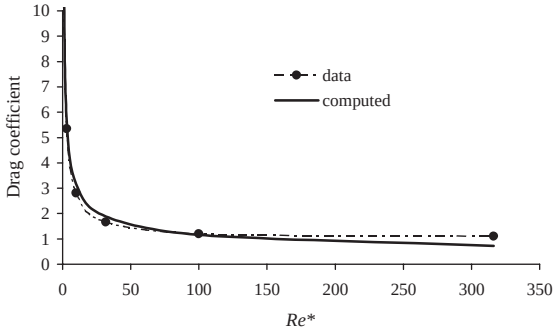

Fig. 5. Results from the C_D formula Eq. (5) compared to data from Tritton [10].

becomes

$$\Delta\rho[\mathrm{kg\ m^3}] \approx 10^{-3}(0.802 - 0.002T)C_0[\mathrm{mg\ l^{-1}}]. \quad (10)$$

Setting Δz in Eq. (8) proportional to the water depth h ($\Delta z \approx h/2$), assuming that a certain fraction (f) of the work done according to Eq. (7) will be spent on vertical mixing, Eq. (8), and expressing density differences by Eq. (10) the following tentative criterion is obtained after rearrangement

$$C_{\max}[\mathrm{mg\ l^{-1}}] = \frac{10^6}{(0.802 - 0.002T[^\circ\mathrm{C}])} \times 8\frac{n\Delta L v}{Bhg\Delta t} f(0.52 + 0.843 Re^{*0.61}), \quad (11)$$

with f a coefficient of proportionality and ΔL the distance between inflow and measuring cross-sections (for the laboratory experiments reported here: 34.15 m).

The series of experiments conducted with artificial vegetation but without wind (Tables 1 and 2) identified two situations that could be termed (or were close to) borderline cases of density stratification, i.e. one between the respective concentrations of Runs 6 and 7, and another close to Run 15. The respective experimental set-ups differed from each other mainly with respect to stem density, all other parameters being fully or nearly identical. Limiting sodium chloride concentrations after initial mixing were found to be some 135 mg l^{-1} (between the 127.4 mg l^{-1} of Run 6 and the 139.7 mg l^{-1} of Run 7) for 12.8 stems m^{-2} and around 70 mg l^{-1} for ca. 7 stems m^{-2}. The latter limiting concentration is slightly below that of Run 15 (with the breakthrough curves shown in Fig. 6), 74 mg l^{-1}, as Run 15 shows slightly larger deviations of the zeroth moments, +23%/−36%, than corresponds to the definition of a borderline case used here, i.e. roughly between ±15% and ±30%. The data for both borderline situations were used to obtain estimates for the coefficient f needed to evaluate Eq. (11) above. For $C_{\max} \approx 135$ mg l^{-1} and 12.8 stems m^{-2} (655 stems in total along $\Delta L = 34.15$ m) one obtains a coefficient $f \approx 0.049$, and for $C_{\max} \approx 70$ mg l^{-1} and about 7.0 stems m^{-2} (356 stems in total along the same ΔL) the estimate is $f \approx 0.047$. Clearly, these two figures agree well, and, thus, a reasonable estimate for f appears to be 0.048.

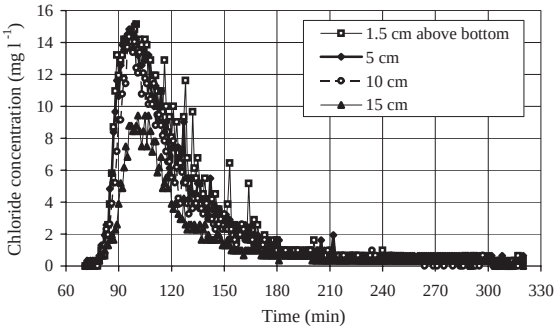

Fig. 6. Measured BTCs, Run 15.

Adapting Eq. (11) to changes in flow rate and Reynolds numbers is difficult and somewhat uncertain on the basis of the available data set. Very rough estimates of $C_{\max}$ made for Run 8 (order of magnitude of some 20 mg l^{-1}), and Run 16 (with $C_{\max}$ probably of the order 10 mg l^{-1}) permit an equally rough estimate of f by: $f \approx 0.0005\ Re^* - 0.027$. The very tentative nature of this relationship must, however, be noted. A plot of dimensionless maximum concentration versus stem Reynolds number Re^* defined by

$$c_{\max} = C_{\max}\frac{Bhg\Delta t}{\Delta L v n}\frac{0.802 - 0.002T}{10^6}. \quad (12)$$

is displayed in Fig. 7.

As mentioned in the previous section, three tracer experiments were run with simultaneous wind shear, i.e. Runs 11–13. In all of these cases water depth amounted to 50 cm, Q to 1.61 s^{-1} and stem density was 12.8 m^{-2}. Run 11 was characterized by a wind speed of 2.4 m s^{-1} in main flow direction, measured 10 cm above the water surface. The distribution of streamwise water velocities about midway between inflow and outflow sections in the flume (cross-section P2) can be seen from Fig. 8, with the full markers denoting measuring points near the flume centreline (L2, L2A) and the other two locations being near the sidewalls (L1 left, L3 right). These measuring points were placed halfway between neighbouring arrays of stems, P2 behind a stem and P2A in the gap midway between two (and, thus, in front of a stem of the next array of the staggered grid shown in Fig. 1).

The distribution of streamwise velocities (Fig. 8) indicates an enhancement of flow in downstream direction in the upper half of the vertical profile and a reversal of direction in the lower half. The zeroth moments (Table 2) showed very well mixed conditions without stratification, the breakthrough curves (at all depths) were positively skewed.

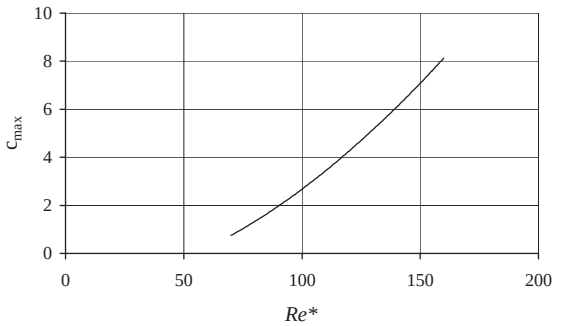

Fig. 7. Dimensionless concentration $c_{\max}$ versus stem Reynolds number Re^*.

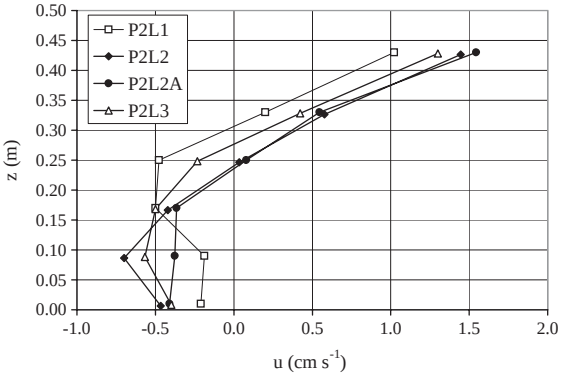

Fig. 8. Velocity distribution at P2 for scenario $Q = 1.61\,\mathrm{l\,s^{-1}}$, 12.8 stems $\mathrm{m^{-2}}$ and $2.4\,\mathrm{m\,s^{-1}}$ wind in main flow direction.

Run 13 is the counterpart of Run 11, with wind speed of $2.4\,\mathrm{m\,s^{-1}}$ against flow direction. The associated velocity profile shows increased downstream velocities near $z = h/2 = 25\,\mathrm{cm}$ and a reversal of flow direction near the water surface, where the effect of wind shear tends to drive water up the flume. Again, well-mixed conditions resulted, this time associated with a near-symmetric breakthrough curve.

The counterpart situation without wind is given by Run 10. In the absence of the mixing action of the wind, density effects were quite strong. Run 12 was analogous to Run 13, but with wind speed against main flow direction of $0.5\,\mathrm{m\,s^{-1}}$ only (in place of the $2.4\,\mathrm{m\,s^{-1}}$ before). In that situation, wind shear was clearly not strong enough to achieve vertical mixing, and the zeroth moments (deviations from the mean of $+56\%/-35\%$) reflected a distinct density stratification.

4. Conclusion

The processes and mechanisms governing the formation of stable density layers in the course of salt tracer experiments in constructed wetland ponds with emergent vegetation were studied. It was found that distinct limits to the injected salt mass exist, if the distortion of breakthrough curves by density effects is to be avoided. Typically, the upper concentration limit to be observed is higher in the presence of emergent plants than without. A tentative criterion was derived to estimate the highest salt concentration after full initial mixing that is not yet associated with strong density effects. Further research to confirm or refine this criterion will be helpful.

Acknowledgements

The research reported here was partly funded by the European Commission under Contract no. EVK1-CT-2000-00065 (PRIMROSE). This support is gratefully acknowledged. The authors also wish to express their thanks to three anonymous reviewers for their constructive comments.

References

[1] Kadlec RH, Knight RL. Treatment wetlands. Boca Raton, FL: CRC Lewis; 1996.
[2] Persson J, Somes NLG, Wong THF. Hydraulics efficiency of constructed wetlands and ponds. Water Sci Technol 1999;40(3):291–300.
[3] Sabir IH, Haldorsen S, Torgersen J, Aleström P, Gaut S, Colleuille H, Pedersen TS, Kitterød N-O. Synthetic DNA tracers: examples of their application in water related studies. TraM'2000 Conference, Proceedings, vol. 262, Liege, IAHS, 2000. p. 159–65.
[4] Smart PL, Laidlaw IMS. An evaluation of some fluorescent dyes for water tracing. Water Resour Res 1977; 13(1):15–33.
[5] Ihme R. The use of overland flow for the purification of runoff water from peat mining areas. PhD thesis, 1994, University of Oulu, Oulu, Finland (in Finnish with abstract in English).
[6] Rutherford JC. River mixing. Chichester, UK: Wiley; 1994.
[7] Hammer DE, Kadlec RH. A model for wetland surface water dynamics. Water Resour Res 1986;22(13):1951–8.
[8] Koskiaho J. Personal Communication, 2001.
[9] Airey PL, Calf GE, Davison A, Morley AW. An evaluation of tracer dilution techniques for gauging of rivers in flood. J Hydrol 1984;74:105–18.
[10] Tritton DJ. Physical fluid dynamics. New York: Oxford University Press; 1991.
[11] Jordanova AA, James CS. Experimental study of bed load transport through emergent vegetation. ASCE J Hydraul Eng 2003;129(6):474–8.
[12] Schiller L, Naumann A. Über die grundlegenden Berechnungen bei der Schwerkraftaufbereitung (On the basic computations in water treatment by settling), Zeitschrift des VDI, vol. 77, 1933 (in German).
[13] Raudkivi AJ. Loose boundary hydraulics. Rotterdam: Balkema; 1998.
[14] Boehrer B, Ilmberger J, Münnich KO. Vertical structure of currents in western Lake Constance. J Geophy Res 2000; 105(C12):28,823–35.
[15] Crowley WP. A global numerical ocean model: Part 1. J Comput Phys 1968;3:111–47.